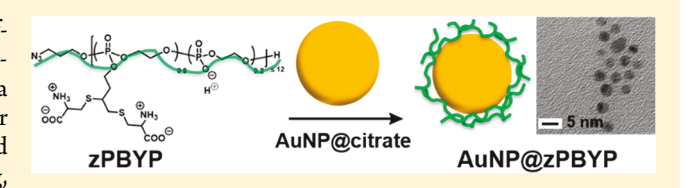
Functional, Degradable Zwitterionic Polyphosphoesters as **Biocompatible Coating Materials for Metal Nanostructures**

Richen Li,^{†,||} Mahmoud Elsabahy,^{†,‡,||} Yue Song,[†] Hai Wang,[†]
[©] Lu Su,[†] Rachel A. Letteri,[†]
Sarosh Khan,[†] Gyu Seong Heo,[§] Guorong Sun,[†] Yongjian Liu,[§]
[©] and Karen L. Wooley*,[†]
[©]

Supporting Information

ABSTRACT: A zwitterionic polyphosphoester (zPPE), specifically L-cysteine-functionalized poly(but-3-yn-1-yloxy)-2-oxo-1,3,2-dioxaphospholane (zPBYP), has been developed as a poly(ethylene glycol) (PEG) alternative coating material for gold nanoparticles (AuNPs), the most extensively investigated metal nanoparticulate platform toward molecular imaging, photothermal therapy, and drug delivery applications. Thiol-



yne conjugation of cysteine transformed an initial azido-terminated and alkynyl-functionalized PBYP homopolymer into zPBYP, offering hydrolytic degradability, biocompatibility, and versatile reactive moieties for installation of a range of functional groups. Despite minor degradation during purification, zPPEs were able to stabilize AuNPs presumably through multivalent interactions between combinations of the side chain zwitterions (thioether and phosphoester groups of the zPPEs with the AuNPs). ³¹P NMR studies in D₂O revealed ca. 20% hydrolysis of the phosphoester moieties of the repeat units had occurred during the workup and purification by aqueous dialysis at pH 3 over ca. 1 d, as observed by the 31P signal of the phosphotriesters resonating at ca. -0.5 to -1.7 shifting downfield to ca. 1.1 to -0.4 ppm, attributed to transformation to phosphates. Further hydrolysis of side chain and backbone units proceeded to an extent of ca. 75% over the next 2 d in nanopure water (pH 5-6). The NMR degradation results were consistent with the broadening and red-shift of the surface plasmon resonance (SPR) observed by UV-vis spectroscopy of the zPPE-coated AuNPs in water over time. All AuNP formulations in this study, including those with citrate, PEG, and zPPE coatings, exhibited negligible immunotoxicity, as determined by cytokine overexpression in the presence of the nanostructures relative to those in cell culture medium. Notably, the zPPE-coated AuNPs displayed superior antifouling properties, as assessed by the extent of cytokine adsorption relative to both the PEGylated and citrate-coated AuNPs. Taken together, the physicochemical and biological evaluations of zPPE-coated AuNPs in conjunction with PEGylated and citrate-coated analogues indicate the promise of zPPEs as favorable alternatives to PEG coatings, with negligible immunotoxicity, good antifouling performance, and versatile reactive groups that enable the preparation of highly tailored nanomaterials for diverse applications.

1. INTRODUCTION

Metal and metal oxide (MO) nanoparticles (NPs) have been extensively explored for imaging, photothermal therapeutic, and drug delivery applications, due to their tunable photophysical properties accessed by feasible syntheses that allow for control over their sizes and morphologies. 1,2 To improve the aqueous stability and decrease the undesirable nonspecific protein adsorption (opsonization) of NPs, both of which are critical factors that affect in vivo fate, various hydrophilic natural and synthetic polymers have been developed and used as coating materials to construct polymer-metal/MO hybrid nanostructures through ligand displacement reactions.^{3,4} Moreover, the incorporation of polymer components also provides facile pathways for introducing cell targeting and/or multimodule imaging functionalities, enabling responsive

properties and enhancing the loading and release performance of NP delivery platforms.

Poly(ethylene glycol) (PEG) represents the "gold standard" polymeric coating material for polymer-metal hybrid nanostructures.⁵ It has been well-established that the PEG can improve NP water solubility, inhibit colloidal aggregation, and reduce the NP opsonization under physiological conditions.^{6,7} However, recent research has indicated that PEGylated biomaterials could lose stealth functions and undergo accelerated blood clearance by mononuclear phagocyte system

Special Issue: Zwitterionic Interfaces: Concepts and Emerging Applications

Received: June 15, 2018 Revised: September 3, 2018 Published: October 22, 2018

Departments of Chemistry, Chemical Engineering, and Materials Science & Engineering, Laboratory for Synthetic-Biologic Interactions, Texas A&M University, College Station, Texas 77842, United States

[‡]Department of Pharmaceutics, Faculty of Pharmacy, Assiut University, 71515 Assiut, Egypt

[§]Department of Radiology, Washington University, St. Louis, Missouri 63110, United States

(MPS) organs after repeated doses due to the production of anti-PEG antibodies by the immune system. ⁸⁻¹⁰ Additionally, conventional telechelic PEGs are nonbiodegradable and lack feasibility for introduction of multiple functional moieties. Therefore, the development of alternative coating materials that provide comparable stabilization and stealth capabilities, evade recognition by the immune system, offer degradability, and impart functionalizable groups is highly desirable for nanoscopic polymer—metal hybrid biomaterials.

Zwitterionic antifouling polymers, e.g., poly(carboxybetaine) (PCB), 11 poly(phosphorylcholine), 12,13 and poly-(sulfobetaine), 14 are potential alternatives to PEG-based coatings, as they are highly resistant to nonspecific protein adsorption. 15 However, our previous results showed that, despite the comparable in vivo stealth properties of PCB to PEG, in certain circumstances, PCB-coated polymeric NPs could exhibit elevated immunotoxicity in comparison with their PEGylated analogues. 16 Biodegradable polymers, such as polyesters, ¹⁷ polyphosphoesters (PPEs), ^{18–20} and poly(glucose carbonate), ²¹ have been studied as promising materials for biomedical applications, which reduce the potential for longterm accumulation and associated adverse effects. Our group has developed degradable zwitterionic polymers, including PPE²² and poly(glucose carbonate), 23,24 to address the immunotoxicity issues.²⁵ Interestingly, polymeric NPs with L-cysteine-functionalized, degradable zwitterionic PPE (zPPE)based shells^{22,26,27} exhibited noticeably decreased immunotoxicities, particularly after shell cross-linking. On the basis of these results, we hypothesized that the utilization of zPPEs as coating materials for metal NPs would enable low immunotoxicity of resulting hybrid NPs while maintaining the favorable antifouling properties of PCB.²⁸ Moreover, the cysteine-derived carboxylic acids and amines in the zPPE corona provide opportunities for cross-linking to enhance the rigidity and stability of the composite nanomaterials.

In this report, a degradable zPPE, namely L-cysteinefunctionalized poly(but-3-yn-1-yloxy)-2-oxo-1,3,2-dioxaphospholane (zPBYP), was synthesized and explored as a PEGalternative coating material for gold NPs (AuNPs), the most extensively investigated metal nanoparticulate platform toward molecular imaging, photothermal therapy, and drug delivery applications.²⁹ Although the utilized zPBYP experienced minor amounts of degradation during the purification process, its capabilities of stabilizing AuNPs, avoiding long-term accumulation by further degradation, realizing minimal immunotoxicity, and decreasing cytokine adsorption relative to AuNPs coated with PEG and citrate were demonstrated. Our investigation also supported the observation that the ultrasmall gold nanoclusters (AuNPs with hydrodynamic diameter <10 nm) could be potential platforms for in vivo diagnostic and theranostic applications.

2. EXPERIMENTAL SECTION

Materials and Methods. Dichloromethane (DCM) and *N,N*-dimethylformamide (DMF) were purified by a solvent purification system (J. C. Meyer Solvent Systems, Laguna Beach, CA). Nanopure water (18 M Ω ·cm) was acquired from a Milli-Q water filtration system (Millipore Co.). Phosphate-buffered saline (PBS) was purchased as a 10× solution from VWR and diluted to a concentration of 1× in nanopure water. Thioctic acid-terminated PEG (TA-PEG-OMe, 750 Da) was purchased from Quanta BioDesign, Ltd. (Plain City, OH). Other reagents were used as received from Sigma-Aldrich, Co. (St. Louis, MO) unless otherwise noted. Dialysis membrane tubing with a molecular weight cutoff

(MWCO) of 3.5 kDa was purchased from Spectrum Laboratories, Inc. (Rancho Dominguez, CA) and soaked for 5 min in nanopure water at room temperature (rt) before use.

Characterization. ¹H NMR, ¹³C NMR, and ³¹P NMR spectra were acquired on a Varian Inova 500 spectrometer interfaced to a UNIX computer using VnmrJ software. Chemical shifts in the ¹H NMR and ¹³C NMR spectra were referenced to the residual solvent resonance signals, while those in the ³¹P NMR spectra were referenced to an external standard, 85% H₃PO₄ in D₂O. FT-IR spectra were recorded on an IR Prestige 21 system (Shimadzu Corp.), equipped with an attenuated total reflectance (ATR) accessory and analyzed using IRsolution version 1.40 software. Ultraviolet—visible (UV—vis) spectroscopy measurements were performed on a Shimadzu UV-2550 spectrophotometer.

Size exclusion chromatography (SEC) eluting with DMF was conducted on a Waters Chromatography, Inc. (Milford, MA) system equipped with an isocratic pump (model 1515), a differential refractometer (model 2414), and a four-column set, including a 5 μ m Guard column (50 × 7.5 mm), a Styragel HR 4 5 μ m DMF column (300 \times 7.5 mm), a Styragel HR 4E 5 μ m DMF column (300 \times 7.5 mm), and a Styragel HR 2.5 μ m DMF column (300 \times 7.5 mm). The system was equilibrated at 50 °C in prefiltered DMF containing 0.05 M LiBr with the flow rate set to 1.00 mL/min. Data collection and analysis were performed with Discovery32 version 1.039.000 software (Precesion Detectors, Inc.). Molecular weights were determined relative to polystyrene standards (615-442800 Da) purchased from Polymer Laboratories, Inc. (Amherst, MA), Polymer solutions were prepared at a concentration of ca. 3 mg/mL with 0.05 vol % toluene added as a flow marker, and an injection volume of 200 μL was used.

Thermogravimetric analysis (TGA) was performed under an Ar atmosphere using a Mettler-Toledo model TGA/DSC 1 with a heating rate of 10 °C/min. Glass transitions $(T_{\rm g})$ were measured by differential scanning calorimetry (DSC) on a Mettler-Toledo DSC822 (Mettler-Toledo, Inc., Columbus, OH) under $\rm N_{2(g)}.$ DSC measurements were performed with a heating rate of 10 °C/min and analyzed using Mettler-Toledo STARe version 10.00 software. The $T_{\rm g}$ was taken as the midpoint of the inflection tangent of the second heating scan.

Electrospray ionization mass spectrometry (ESI-MS) experiments were performed using a Thermo Scientific LCQ-DECA instrument. The sample was directly infused at a flow rate of 6 μ L/min. The spray voltage was set to -4.5 kV, and the sheath gas and auxiliary gas flow rates were set to 50 and 10 au, respectively. The transfer capillary temperature was held at 250 °C. Xcalibur 2.0 software was used for data acquisition and processing.

Inductively coupled plasma mass spectrometry (ICP-MS) was performed on a PerkinElmer SCIEX ICP mass spectrometer ELAN DRC II equipped with a high-speed quadrupole, a dynamic reaction cell (DRC), and axial field technology (AFT) to eliminate polyatomic interference, using 1% HNO₃ as the matrix and rhodium as the internal standard. The amount of Au in each sample was determined by ICP-MS after dilution with 1% HNO₃.

High-resolution scanning transmission electron microscopy (STEM) was conducted on a FEI Tecnai G2 F20 FE-TEM coupled with energy-dispersive X-rays (EDX), operating at a voltage of 200 kV and equipped with a Gatan CCD camera. Samples for TEM were prepared as follows: $10~\mu L$ of a dilute NP solution in nanopure water was deposited onto a carbon-coated copper grid, and after 1 min, excess solution was quickly wicked away by a piece of filter paper, and the samples were left to dry under ambient conditions overnight.

Dynamic light scattering (DLS) measurements were conducted using a Delsa Nano C instrument from Beckman Coulter, Inc. (Fullerton, CA) equipped with a laser diode operating at 633 nm. Scattered light from 0.5 mL samples in a disposable polystyrene cell (0.9 mL capacity) was detected at 165° and averaged over 70 accumulations. The photomultiplier aperture and attenuator were adjusted automatically to obtain a photon count rate of ca. 10 kcps. The particle size distribution and distribution averages (i.e., the intensity-, volume-, and number-average hydrodynamic diameters)

were calculated using CONTIN particle size distribution analysis routines in Delsa Nano 2.31 software. All measurements were repeated 10 times.

Atomic force microscopy (AFM) was performed using a Multimode 8 system (Bruker) in PeakForce tapping mode using a ScanAsyst-Air Silicon Nitride probe ($k=0.4\,$ N/m, $f_0=70\,$ kHz, Bruker). AFM images were processed with Nanoscope Analysis 8.15 software (Bruker). Samples were prepared by deposition of a solution of nanoparticles in nanopure water ($50\,\mu\text{L}$, $0.2\,$ mg/mL) onto freshly cleaved mica substrates. After 1 min, excess solution was wicked away by a piece of filter paper, and the mica surface was allowed to dry in air.

Synthetic Protocols. Synthesis and characterization of the cyclic phosphotriester monomer BYP was performed according to a previously reported procedure. 30

Synthesis of PBYP. A solution of BYP (0.9910 g, 5.631 mmol) and 3-azido-1-propanol (48.4 mg, 0.479 mmol) in anhydrous DCM (2 mL) was transferred via syringe into a flame-dried vial equipped with a stir bar and rubber septum under $N_{2(g)}$ at rt. A solution of organocatalyst 1,8-diazabicyclo [5.4.0] undec-7-ene (DBU) (82.3 mg, 0.592 mmol) in anhydrous DCM (0.2 mL) was injected quickly into the vial. After the contents were stirred for 20 min, the reaction vial was opened to air, and the reaction was quenched by addition of excess acetic acid. An aliquot of the reaction mixture was withdrawn and diluted with CDCl₃ to determine the BYP monomer conversion using 31P NMR spectroscopy by comparison of the relative integrations of the peaks at 17.97 and between -0.20 and -1.89ppm, corresponding to cyclic and ring-opened phosphoester resonances, respectively. PBYP was purified by precipitation from DCM into diethyl ether and then dried under a vacuum to afford a colorless liquid (893.6 mg, 85% yield). ¹H NMR (500 MHz, CDCl₃): δ 4.47–3.93, 3.83–3.66 (m, POCH₂CH₂O, POCH₂CH₂C≡CH, $N_3CH_2CH_2CH_2$), 3.42 (t, N_3CH_2 , J = 5.0 Hz), 2.64–2.51 (br, $CH_2C \equiv CH$), 2.18-2.02 (br, $CH_2C \equiv CH$), 1.92 (q, $N_3CH_2CH_2$, J =5.0 Hz) ppm. ¹³C NMR (126 MHz, CDCl₃): δ 79.56, 70.84, 66.46, 65.82, 65.02, 47.58, 29.63, 20.64 ppm. ³¹P NMR (202 MHz, CDCl₃): δ -0.2 to -1.89 ppm. FT-IR (ATR) 3700-3100, 3100-2700, 2100, 1711, 1647, 1456, 1375, 1271, 1230, 1009, 964, 800, 733 cm⁻¹. $T_g =$ -37 °C. TGA in Ar: 170-310 °C, 57% mass loss; 310-500 °C, 14% mass loss, 29% mass remaining at 500 °C. SEC (0.01 M LiBr in DMF, PS standards): $M_n = 14.9 \text{ kDa}$, D = 1.22.

Postpolymerization Modification of PBYP with L-Cysteine via Thiol-Yne Reaction To Afford Zwitterionic PBYP (zPBYP). PBYP (941.8 mg, 5.1 mmol alkyne groups), L-cysteine (9.0595 g, 51.580 mmol), 2,2-dimethoxy-2-phenylacetophenone (DMPA, 395.0 mg, 1.541 mmol), and concentrated HCl (11.65 M, 4.4 mL, 51 mmol) were dissolved in N,N-dimethylacetamide (DMAc, 35 mL), deoxygenated under $N_{2(g)}$ for 10 min, and irradiated under UV light (365 nm) for 2.5 h with stirring. The resulting solution was transferred to dialysis tubing (MWCO 3.5 kDa) and dialyzed against nanopure water adjusted to pH 3 with HCl at 4 °C for 1 d to remove excess thiol and photoinitiator. The solution was then lyophilized to afford zPBYP as a white solid (1.3318 g, 61% yield). ¹H NMR (500 MHz, D_2O): δ 4.59–4.18 (br, $N_3CH_2CH_2CH_2$, $POCH_2CH_2O$, POCH₂CH₂CH), 4.18-3.91 (br, CH₂CH(NH₃)COOH, POCH₂CH₂CH), 3.91-3.70 (POCH₂CH₂ in the anionic repeat units), 3.51 (t, N_3CH_2 J = 5.0 Hz), 3.40-2.61 (br, $SCHCH_2S$, SCHCH₂S, CH₂SCHCH₂S, SCHCH₂SCH₂), 2.40–2.14, 2.06–1.72 (br, N₃CH₂CH₂, POCH₂CH₂CH) ppm. ¹³C NMR (126 MHz, CDCl3): δ 172.06, 68.02, 67.21, 66.35, 65.22, 64.50, 53.40, 47.28, 36.61, 36.21, 31.49, 29.03 ppm. ³¹P NMR (202 MHz, CDCl₃): δ 1.10 to -1.70 ppm. FT-IR (ATR) 3140-2780, 2670, 2460, 1780, 1655, 1593, 1514, 1472, 1362, 1285, 1207, 1097, 991, 912, 843, 760 cm⁻¹ $T_g = -64$ °C. TGA in Ar: 150–200 °C, 11% mass loss; 200–400 °C, 46% mass loss, 43% mass remaining at 500 °C.

Synthesis of Citrate-Coated AuNP (AuNP@citrate). Into a 20 mL glass vial equipped with a stir bar, nanopure water (5 mL), HAuCl₄ (10 mM, 500 μ L), and sodium citrate solution (20 mM in nanopure water, 500 μ L) were added and allowed to stir. ³¹ Ice-cold, freshly prepared sodium borohydride solution (20 mM in nanopure

water, 1 mL) was then quickly added to the mixture while vigorously stirring at rt. The solution turned pink after a short time, indicative of the formation of AuNPs, and was stirred for an additional 0.5 h. The AuNPs were then purified by centrifugal filtration (MWCO 10 kDa) with nanopure water three times at 3500 rpm.

Preparation of zPBYP-Coated AuNP (AuNP@zPBYP). In a typical reaction, zPBYP (1.0 mg) was dissolved in 1× PBS (pH = 7.4, 1 mL). A solution of AuNP@citrate (2 mL, 0.14 mg/mL Au as determined by ICP-MS) in nanopure water was then added dropwise into the solution of zPBYP using a syringe pump over 5 min while stirring. The reaction mixture was stirred for 3 h, and the polymer-coated NPs were purified by centrifugal filtration (MWCO 10 kDa) with nanopure water three times at 3500 rpm.

Preparation of PEG-Coated AuNPs (AuNP@PEG). In a typical reaction, TA-PEG-OMe (1.0 mg, 1.3 μ mol) was dissolved in 1× PBS (pH = 7.4, 1.0 mL). A solution of AuNP@citrate (2 mL, 0.14 mg/mL Au) was then added dropwise into the solution of TA-PEG-OMe using a syringe pump over 5 min while stirring. The reaction mixture was stirred for 3 h, and the PEG-coated NPs were purified by centrifugal filtration (MWCO 10 kDa) with nanopure water three times at 3500 rpm.

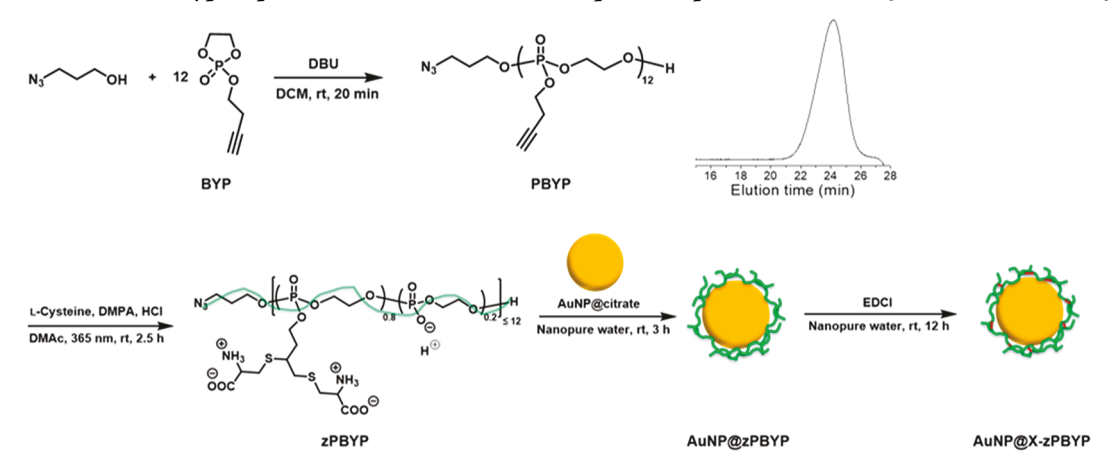
Preparation of Shell Cross-Linked zPBYP-Coated AuNP (AuNP@X-zPBYP). To a solution of AuNP@zPBYP (2 mL, 0.14 mg/mL Au, 0.44 μmol of carboxylic acids, 0.44 μmol of amines), a solution of 1-[3-(dimethylamino)propyl]-3-ethylcarbodiimide methiodide (EDCI, 650 μL, 0.10 mg/mL in water) was added. The reaction was allowed to stir overnight at rt, and the cross-linked nanostructures were purified by centrifugal filtration (MWCO 10 kDa) with nanopure water three times at 3500 rpm.

Hydrolytic Degradation of zPBYP. In a typical study, a lyophilized sample of zPBYP (15.1 mg) was dissolved in D₂O (0.4 mL) and transferred into an NMR tube. The sample was maintained in a New Brunswick Innova 44 incubator shaker (37 °C, 60 rpm) and characterized by ³¹P NMR to monitor the degradation progress at predetermined times (0 h and 1, 2, 3, 4, and 6 d). The study was repeated in triplicate. After 6 d, an aliquot of the sample was diluted with methanol and further characterized by ESI-MS for identification of small-molecule degradation products. The remaining sample was dialyzed against nanopure water in dialysis tubing (MWCO 1 kDa), followed by lyophilization to determine the amount of residual material retained in the dialysis tubing.

Degradation Study of AuNP@zPBYP in Comparison to AuNP@citrate, AuNP@PEG, and AuNP@X-zPBYP. In a typical study, a solution of AuNP@zPBYP was kept in the incubator shaker (37 °C, 60 rpm) and characterized by UV—vis spectroscopy at predetermined times (0, 1, 2, 4, 6, and 14 d). Similarly, the stabilities of AuNP@citrate, AuNP@PEG, and AuNP@X-zPBYP in the incubator shaker were evaluated by monitoring the surface plasmon resonance (SPR) over 14 d.

Cytokine Multiplex Assay. The multiplex assay was performed as reported previously.²⁸ RAW 264.7 (2 \times 10⁴ cells/well) mouse macrophages were plated in a 96-well plate in Dulbecco's Modified Eagle Medium (DMEM) (10% fetal bovine serum and 1% penicillin/ streptomycin) and incubated at 37 °C and 5% CO2 for 24 h. The medium was then replaced with fresh medium 1 h prior to the addition of 20 µL of each of the samples (medium (control), AuNP@ citrate, AuNP@zPBYP, AuNP@PEG, and AuNP@X-zPBYP (5 µg/ mL Au in each sample)). After a 24 h incubation, the supernatants were collected and centrifuged for 10 min at 13000 rpm. Serial dilutions of cytokine standards (Bio-Rad Laboratories, Inc., Hercules, CA) were prepared in cell-culture medium to generate a calibration curve with which to determine cytokine concentration. The cytokine standard and cells treated with culture medium (control, 50 μ L) and NPs (50 μ L) were incubated with antibody-conjugated magnetic bead solution (50 μ L) for 30 min in the dark. After washing, the detection antibody solution (50 μ L) was added to the wells, and they were incubated in the dark for 30 min under continuous shaking (300 rpm). After washing, a streptavidin-phycoerythrin solution (50 μ L) was added to each well, and they were incubated while being protected from light for 10 min under continuous shaking (300 rpm).

Scheme 1. Synthesis of PBYP Followed by Post-Polymerization Modification via a Thiol—Yne Click Reaction with L-Cysteine to Yield the Zwitterionic Polyphosphoester zPBYP and the Subsequent Preparation of AuNP@zPBYP and AuNP@X-zPBYP



^aInset: SEC trace of PBYP in DMF.

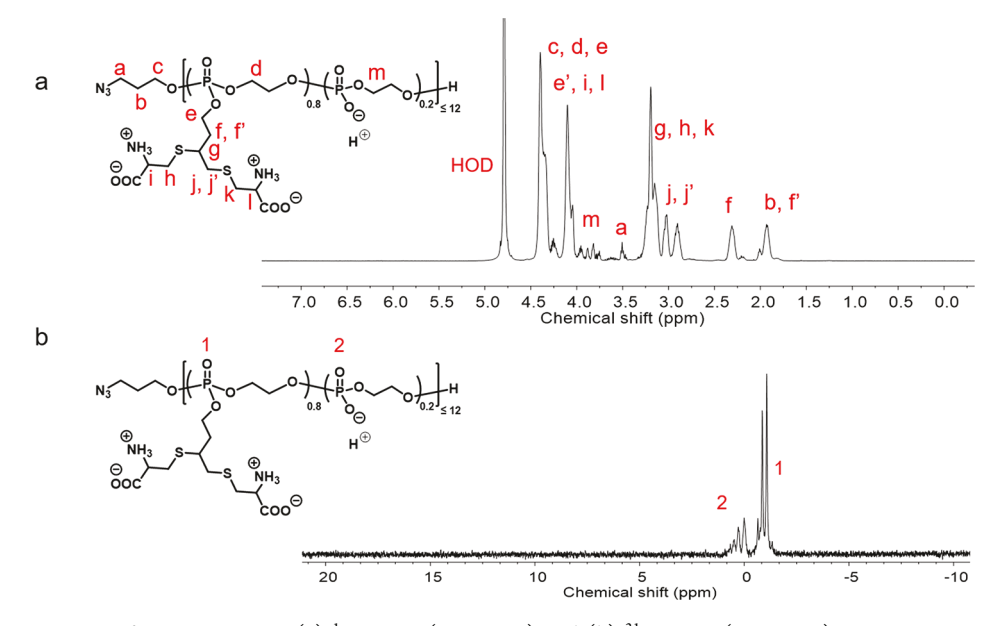


Figure 1. NMR spectroscopy of zPBYP in D₂O: (a) ¹H NMR (500 MHz) and (b) ³¹P NMR (202 MHz) spectra.

Finally, after several cycles of washing and resuspension in the assay buffer and shaking, the expression of the mouse cytokines, interleukin (IL)-1 α , IL-1 β , IL-2, IL-3, IL-4, IL-5, IL-6, IL-9, IL-10, IL-12 (P40), IL-12 (P70), IL-13, IL-17, eotaxin, granulocyte-colony-stimulating factor (G-CSF), granulocyte macrophage-colony stimulating factor (GM-CSF), interferon- γ (IFN- γ), keratinocyte-derived chemokine (KC), monocyte chemotactic protein (MCP)-1, macrophage inflammatory protein (MIP)-1 α , MIP-1 β , regulated upon activation normal T-cell expressed and presumably secreted (RANTES), and tumor necrosis factor- α (TNF- α), were measured immediately using a Bioplex 200 system equipped with high-throughput fluidics (HTF) and a Pro II Wash station, and the data were analyzed using Bioplex Data Pro software. Cytokine expression was reported relative to that by cells in the culture medium.

Cytokine Adsorption Assay. Adsorption of the mouse cytokines, IL-1 α , IL-1 β , IL-2, IL-3, IL-4, IL-5, IL-6, IL-9, IL-10, IL-12 (P40), IL-12 (P70), IL-13, IL-17, Eotaxin, G-CSF, GM-CSF, IFN- γ , KC, MCP-1, MIP-1 α , MIP-1 β , RANTES, and TNF- α , onto the AuNPs was measured using a Bioplex 200 system equipped with HTF and a Pro II Wash station. Specific concentrations of the cytokine standards were determined either in cell culture medium (DMEM) or when mixed with the various NPs (5 μ g/mL) in the same medium, as described

previously. 16,32 The values are reported in Figure 6 as the ratio of the cytokine concentration in the cytokines/NP mixtures to that in samples without NPs treated and subjected to the same rinsing procedures.

3. RESULTS AND DISCUSSION

Design and Synthesis of the Functional, Degradable Zwitterionic Polyphosphoester zPBYP. The zPBYP was designed as an alternative AuNP coating material to PEG, with zwitterions in the side chains to prevent biofouling and undesired immune system responses and an azide group at the chain end to enable attachment of drugs, targeting moieties, and imaging agents (Scheme 1). A PPE backbone was selected due to its previously reported biocompatibility, degradability, and chemical versatility. The chain length was set to be relatively short, with a target degree of polymerization (DP_n) of 12, to allow comparison with the previously reported TA-PEG-OMe (DP_n = 12), which stabilized ultrasmall NPs with number-average hydrodynamic diameters $(D_{h(number)}) < 10$ nm postulated to promote effective renal clearance in vivo. The

azide group on the chain end, while not utilized in this work, provides opportunities for further modification of the polymer via azide—alkyne click reactions to expand the utility and scope of the NPs.

The alkyne-functionalized homopolymer PBYP was synthesized by rapid organocatalyzed ring-opening polymerization (ROP) of the cyclic phosphotriester monomer BYP at rt in DCM with 3-azidopropanol as the initiator and DBU as the organocatalyst (Scheme 1). After 20 min, the reaction was quenched by addition of excess acetic acid. The ³¹P NMR spectrum of the reaction aliquot showed almost complete conversion of the single cyclic monomer signal (resonating at 18.0 ppm) to several polymer ³¹P resonance frequencies (between -0.2 to -1.9 ppm) (Figure S1). Size exclusion chromatography (SEC) of the purified product (Scheme 1 inset) revealed a monomodal molar mass distribution with relatively narrow dispersity (D = 1.22), consistent with the controlled character of organocatalyzed ROP to yield welldefined polymers. The number-average molar mass (M_n) and degree of polymerization (DP_n) were calculated from the ¹H NMR spectrum of PBYP (Figure S2) by comparing the integration of the proton resonances from the initiator (3.4 ppm) with those of the polymer side chain proton resonances (2.6-2.5 ppm).

The zwitterionic polymer, zPBYP, was synthesized by postpolymerization modification of PBYP via photoinitiated thiol-yne click reaction of PBYP with excess L-cysteine (10 equiv relative to alkyne groups), as shown in Scheme 1. The similar solubilities of L-cysteines and zPBYP in a variety of solvents rendered purification by precipitation unfeasible; therefore, the reaction mixture was dialyzed against water acidified with HCl (pH = 3) at 4 °C for 1 d to remove excess thiol and photoinitiator and then lyophilized to afford zPBYP as a white solid in 61% yield. The appearance of signals for protons adjacent to the L-cysteine sulfur atom, resonating between 3.5 and 2.8 ppm, and the disappearance of the alkyne proton resonances (2.2-2.0 ppm) in the ¹H NMR spectrum indicated quantitative consumption of the alkynes (Figure 1a). Following purification of zPBYP, the appearance of resonances between 1.1 and -0.4 ppm in the ³¹P NMR spectrum (Figure 1b) indicated partial degradation despite measures to inhibit degradation, i.e., acidification of the dialysis solution to protonate the cysteine amines to reduce their nucleophilicity. Nevertheless, given that the polymer was obtained in ca. 60% yield, which would presumably be substantially lower if the polymer had degraded into oligomers and been removed by dialysis, the degradation is assumed to occur predominantly by cleavage of side chains or near the chain ends. The extent of degradation was determined to be ca. 20% by comparing the integration of resonances of the phosphate groups between 1.1 and -0.4 ppm to the total integration of phosphorus resonances, i.e., from 1.1 to -1.7 ppm. The multiple resonances from 4.0 to 3.7 ppm in the ¹H NMR spectrum were assigned to the backbone protons in the anionic repeat units, consistent with our previously reported NMR spectroscopy results on PPE ionomers.³⁴ While degradation of zPBYP during purification was difficult to avoid, the presence of anionic groups was not anticipated to be detrimental to the stabilization of AuNPs. Taken together, the introduction of large amounts of zwitterionic L-cysteine groups onto biocompatible and degradable PPEs yielded promising PEGalternative coating materials, which were then investigated for

their ability to stabilize AuNPs and reduce immunotoxicity (vide infra).

Synthesis of AuNPs with Different Coatings. Citrate-coated AuNPs (AuNP@citrate) were prepared according to literature procedures³¹ in which strong reducing agents are added to solutions of gold salts with stabilizing agents to produce small-sized AuNPs. In a typical reaction, HAuCl₄ and sodium citrate were mixed in nanopure water followed by the addition of a freshly prepared solution of NaBH₄ in nanopure water (cooled in an ice bath prior to use) under vigorous stirring. The solution was then allowed to stir at rt for 30 min before purification by centrifugal filtration. Consistent with literature reports, ^{35,36} a characteristic absorption peak was observed in the UV—vis spectrum (Figure 2, black trace) of

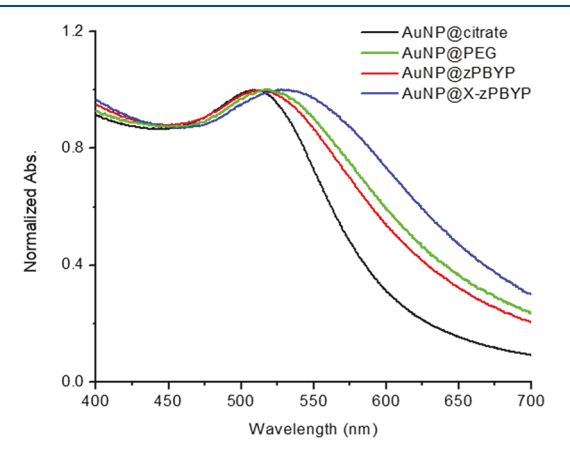


Figure 2. Characterization of coated AuNPs in nanopure water by UV—vis spectroscopy.

AuNP@citrate at 510 nm, corresponding to the SPR of AuNPs. TGA showed minimal mass loss for AuNP@citrate upon heating up to 500 $^{\circ}$ C under Ar (Figure S5), which is also consistent with literature reported results on citrate-coated AuNPs 37

Polymer-coated AuNPs, AuNP@zPBYP and AuNP@PEG, were prepared by addition of AuNP@citrate dropwise into polymer solutions while stirring. The reaction mixtures were stirred for 3 h at rt before purification by centrifugal filtration. While PEG (TA-PEG-OMe) was anchored to the AuNPs by bidentate ligation of TA moieties at the chain end to the AuNP surface, zPBYP is postulated to displace citrate ligands and coat AuNPs by multivalent interactions between the thioether, carboxylic acid/carboxylate, and amine/ammonium groups³ of the side chains and Au atoms on the NP surface. The UVvis spectra of both AuNP@zPBYP and AuNP@PEG showed broadening and a small red-shift of the SPR peak (to 514 and 518 nm, respectively) relative to AuNP@citrate (Figure 2). In contrast to the negligible mass loss observed upon heating AuNP@citrate, the polymer coatings of AuNP@zPBYP and AuNP@PEG accounted for 26% and 18% of the total mass, respectively, on the basis of TGA (Figure S5 and S6). It is noteworthy that the AuNP@citrate composites destabilized upon freezing, and black solids were observed after lyophilization that could no longer be dissolved in aqueous solution. In contrast, lyophilized AuNP@zPBYP and AuNP@ PEG redispersed readily in aqueous solution. These results indicated superior AuNP stabilization by the zPBYP and PEG coatings relative to citrate, attesting to the potential of these

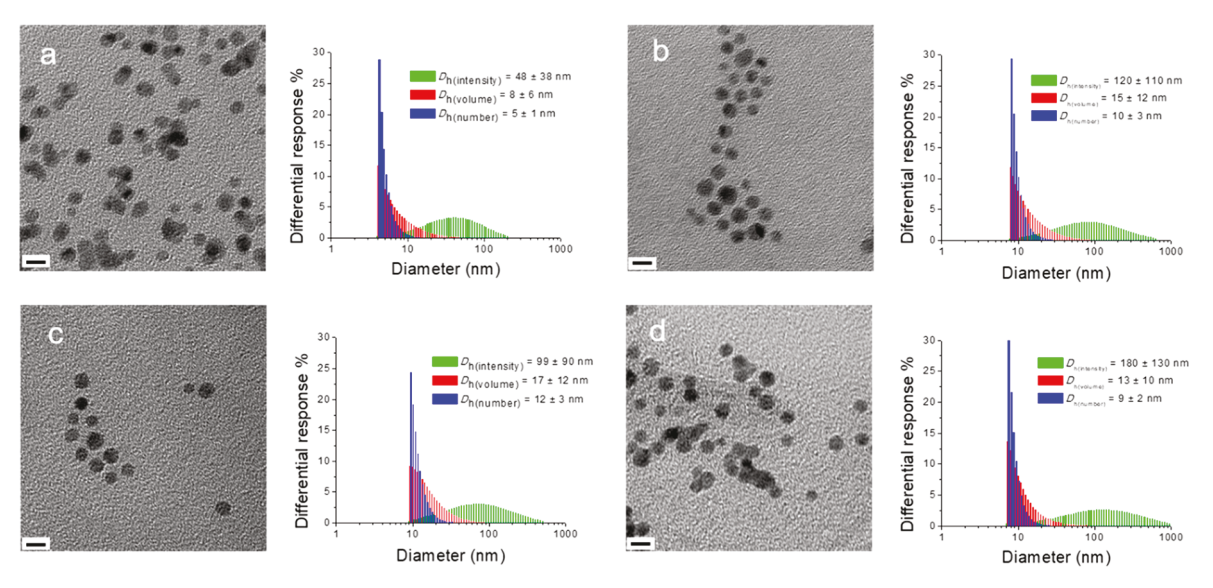


Figure 3. TEM images and DLS size distributions of (a) AuNP@citrate, (b) AuNP@zPBYP, (c) AuNP@PEG, and (d) AuNP@X-zPBYP samples; scale bar = 5 nm. Number-, intensity-, and volume-averaged hydrodynamic diameters were obtained by DLS in nanopure water.

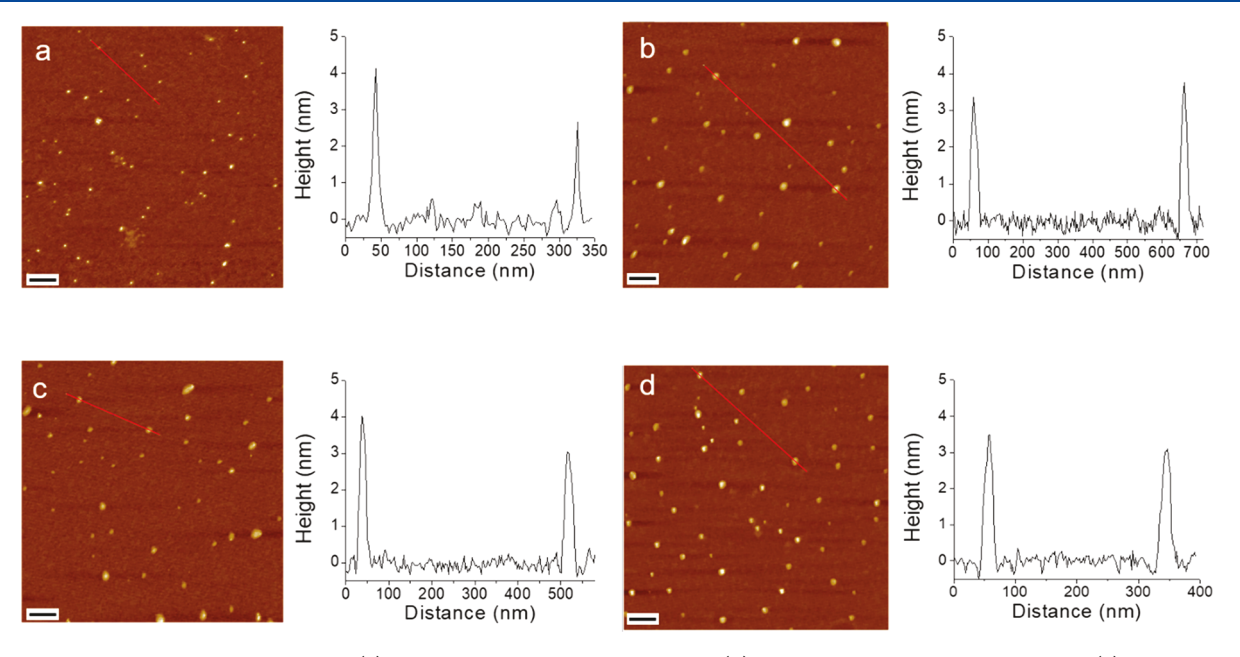


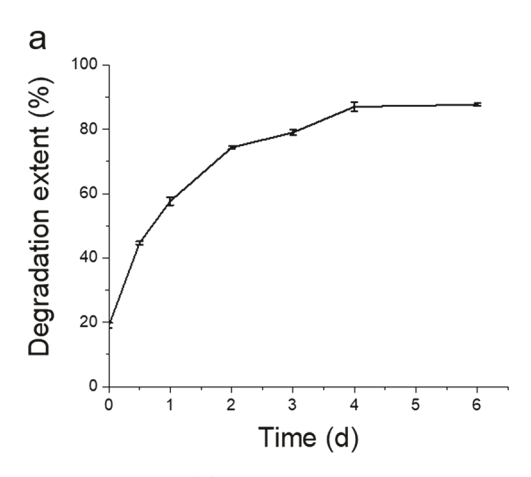
Figure 4. AFM images and height profiles of (a) AuNP@citrate, $H_{\rm av} = 3.3 \pm 0.7$ nm, (b) AuNP@zPBYP, $H_{\rm av} = 3.6 \pm 0.9$ nm, (c) AuNP@PEG, $H_{\rm av} = 3.5 \pm 0.6$ nm, and (d) AuNP@X-zPBYP $H_{\rm av} = 3.4 \pm 0.8$ nm, plotting the height as a function of lateral distance along the red lines in the images. Samples were prepared by drop-casting AuNP solutions onto freshly cleaved mica. Scale bar = 100 nm.

zwitterionic polymers as PEG-alternative coatings to enable storage and transport of therapeutically relevant nanomaterials.

As our previous work demonstrated a remarkable improvement of polymer NP stability and biocompatibility upon cross-linking, ²⁸ AuNPs with cross-linked polymer coatings (AuNP@X-zPBYP) were prepared by adding a solution of EDCI in nanopure water to a solution of AuNP@zPBYP to mediate amidation of the carboxylic and amine groups in the L-cysteine side chains of zPBYP. The solution was allowed to stir overnight before purification by centrifugal filtration with nanopure water. By controlling the stoichiometry of EDCI (12 equiv relative to each polymer chain), ca. half of the reactive functionalities of the polymer coatings were postulated to undergo carbodiimide-mediated amidation to achieve a shell cross-linking extent that has been demonstrated with improved

in vivo blood retention of nanostructures.³⁹ The UV-vis spectrum of AuNP@X-zPBYP showed a broadened and further red-shifted absorption peak (528 nm) with respect to the uncross-linked AuNP formulations (Figure 2), attributed to a certain degree of inter-NP cross-linking to yield larger NPs. Yet, no discernible precipitation was observed from the solution of AuNP@X-zPBYP at 4 °C for over three weeks.

Evaluation of AuNP Formulations by Microscopy and Light Scattering. The sizes of the coated AuNPs were assessed by TEM, DLS, and AFM to obtain complementary information from nanoscale solid-state imaging and insuspension analysis. As depicted in Figure 3, TEM images of AuNP@citrate, AuNP@zPBYP, AuNP@PEG, and AuNP@XzPBYP suspensions showed circular shapes with narrow size distributions and average diameters (D_{av}) of 4.2 ± 0.6 , $3.9 \pm$



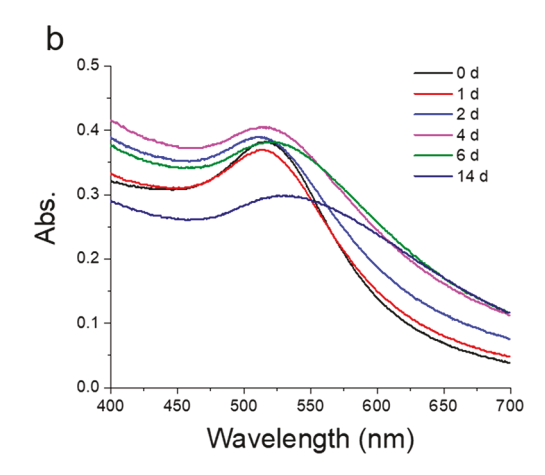


Figure 5. Degradation kinetics of (a) zPBYP in D₂O at 37 °C, evaluated by ³¹P NMR spectroscopy and (b) AuNP@zPBYP, evaluated by UV-vis spectroscopy.

0.7, 4.1 \pm 0.6, and 4.0 \pm 0.6 nm, respectively, counting >50 NPs. Aggregation of NPs on the TEM grid was observed in the AuNP@citrate sample (Figure 3a, left), which likely occurred during sample preparation. In contrast, the increased spacing between the Au cores observed for the AuNP@PEG and AuNP@zPBYP samples is consistent with the larger polymer coatings (Figures 3b,c left), which effectively inhibited aggregation during sample drying on the TEM grid, further attesting to the superior stabilization abilities by these polymer coatings. TEM of the AuNP@X-zPBYP structures (Figure 3d) revealed some aggregation, resulting from either inter-NP cross-linking or aggregation upon drying due to the consumption of hydrophilic zwitterionic moieties during the cross-linking reaction. DLS analyses (Figure 3) revealed unimodal size distributions of all NP samples, indicative of the uniformity of these coating procedures. The numberaverage hydrodynamic diameter (D_{h(number)}) of the AuNP@ citrate nanostructure was determined to be 5 ± 1 nm. After coating with zPBYP or TA-PEG-OMe, the $D_{h(number)}$ of the NPs increased to 10 ± 3 and 9 ± 2 nm, respectively. The similar hydrodynamic diameters of the NPs validate the comparability between the zPBYP and PEG coatings. No significant increase was observed in the $D_{\rm h(number)}$ of AuNP@XzPBYP, indicating that the desired intra-NP shell cross-linking was dominant over inter-NP cross-linking.

AFM revealed globular structures from the AuNP@citrate, AuNP@zPBYP, AuNP@PEG, and AuNP@X-zPBYP samples with similar average heights of 3.3 \pm 0.7, 3.6 \pm 0.9, 3.5 \pm 0.6, and 3.4 ± 0.8 , respectively, counting >50 NPs (Figure 4). Overall, the AFM-measured diameters were greater than the TEM-measured diameters and the AFM-measured heights due to tip effects. However, the larger diameters (ca. 50 nm) of the structures observed in the images of the AuNP@zPBYP, AuNP@PEG, and AuNP@X-zPBYP samples relative to those (ca. 25 nm) of the AuNP@citrate sample are attributed to the spreading of the polymer coatings on the polar mica substrate. Taken together, TEM, DLS, and AFM measurements indicate the successful, uniform coating of AuNPs with citrate and polymers, and these nanocomposites were further investigated to evaluate their immunotoxicity and cytokine adsorption as a function of coating composition in vitro.

Degradation Studies of zPBYP and AuNP@zPBYP. Degradation kinetics of zPBYP were monitored by 31 P NMR spectroscopy in D₂O at 37 $^{\circ}$ C, acquiring spectra at

predetermined times (Figure 5a and S8). These data showed that after 2 d, hydrolysis of side chain and backbone units proceeded to an extent of ca. 75% in nanopure water (pH 5–6). The formation of small-molecule products derived from the side-chain moieties and monomeric repeat units of zPBYP was confirmed by ESI-MS (Figure S9). After the degradation extent reached ca. 90% by 6 d, as determined by ³¹P NMR spectroscopy, the sample was dialyzed against nanopure water to remove small molecule products and lyophilized. Analysis of the material retained in the dialysis membranes indicated that 71 wt % of the polymer still existed as macromolecules after immersion in D₂O for 6 d.

Degradation of AuNPs with different coatings was also evaluated at 37 °C by monitoring changes in the SPR peak by UV-vis spectroscopy. From 0 h to 14 d, the SPR peak of the AuNP@citrate, AuNP@PEG, and AuNP@X-zPBYP did not change appreciably (Figure S10), indicating the relative stability of these NPs. In comparison, the SPR peak of AuNP@zPBYP broadened slightly after 2 d, presumably due to degradation of the un-cross-linked zPBYP coating. Continued monitoring of the un-cross-linked AuNP@zPBYP from 4 to 14 d showed the SPR peak to broaden further and red-shift significantly, indicating aggregation of the NPs (Figure 5b). Small amounts of precipitate were observed after 14 d. These results demonstrate both the degradability of the zPBYP coatings and the effectiveness of shell cross-linking to increase stability. The degradable coatings are expected to be particularly appealing in biomedical contexts by alleviating safety concerns associated with long-term accumulation of nondegradable macromolecular materials.

Evaluation of Immunotoxicity and Anti-Biofouling Properties of Coated AuNP Formulations. The immunotoxicity of the AuNP formulations was evaluated by incubating RAW 264.7 mouse macrophages with various formulations for 24 h, followed by measuring the expression levels of 23 cytokines using a previously established multiplexing assay. The in vitro immunotoxicity was evaluated in terms of cytokine overexpression by cells exposed to NP formulations relative to that in those not exposed to NPs, indicative of the level of inflammatory immune response. No significant overexpression of any of the 23 tested cytokines was observed in the presence of all four AuNP formulations relative to the control (data not shown). These results demonstrated the low immunotoxicity of the coated AuNPs, suggesting the

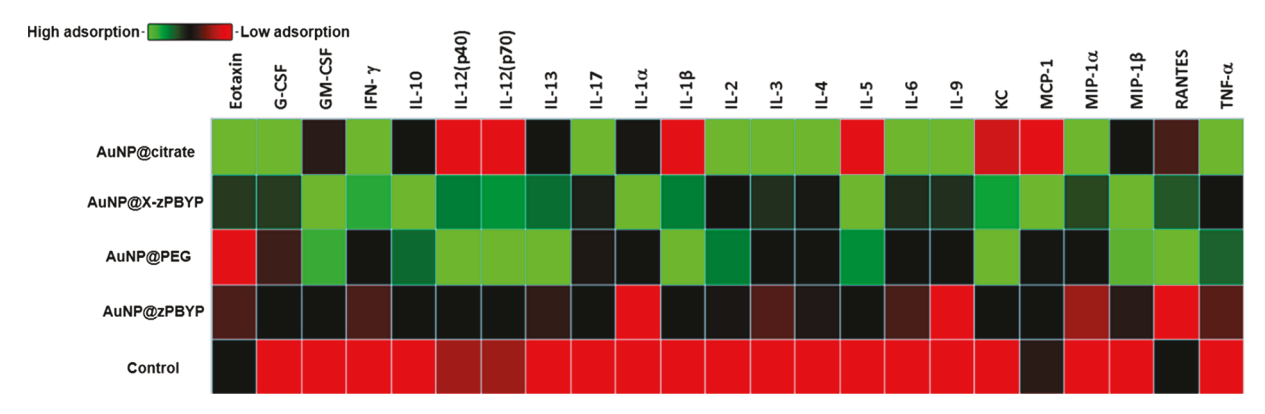


Figure 6. Cytokine adsorption on the coated AuNP formulations, calculated on the basis of apparent concentrations of cytokines measured after incubation with NPs and subsequent rinsing to remove unadsorbed material, as compared to the concentrations in a solution containing no NPs. The figure is the heatmap showing the concentrations of the various cytokines.

biocompatibility of these zPBYP coatings and supporting their viability as alternative coating materials to PEG.

Adsorption of cytokines onto AuNPs was calculated on the basis of apparent concentration of cytokines measured after incubation with NPs and subsequent rinsing steps to remove unadsorbed cytokines as compared to their concentrations in samples subject to the same procedures without NPs. The twodimensional heatmap (values normalized to the control levels) in Figure 6 shows the results of cytokine adsorption assay, where red squares indicate lower cytokine adsorption in heatmap (i.e., from red to green, adsorption becomes higher). Notably, the AuNP@zPBYP formulations exhibited the lowest cytokine adsorption out of all the NP formulations, while reduced adsorption was also measured for AuNP@PEG compared to AuNP@citrate which displayed significant cytokine adsorption. While the cross-linked formulations demonstrated low immunotoxicity and higher stability, they exhibited higher cytokine adsorption compared to their uncross-linked counterparts probably due to the presence of larger NPs as well as the consumption of charged moieties upon cross-linking, rendering the particles more hydrophobic and attractive to biomolecules. Future optimization of AuNP@ X-zPBYP constructs will involve lowering the cross-linking degree to achieve a balance between NP stability and reduced cytokine adsorption.

4. CONCLUSIONS

The zwitterionic PPE, zPBYP, was designed and synthesized to afford a promising alternative to PEG as an AuNP coating material offering hydrolytic degradability, favorable immunotoxicity, and antifouling properties. Organocatalyzed ROP of the cyclic phosphotriester monomer BYP with 3-azidopropanol as the initiator yielded the alkyne-functionalized PPE with a monomodal molar mass distribution. Functionalization of the alkynes in the side chains of the polymer with L-cysteine via thiol-yne click reactions yielded zPPEs. Despite minor degradation of the polymer during purification by dialysis, the installation of large amounts of zwitterions in the side chains yielded highly hydrophilic polymers, which were coated successfully onto AuNPs through multivalent interactions between the thioether, carboxylic acid/carboxylate, and amine/ammonium groups of the polymer side chains and the Au surface of the NPs. AuNP@citrate was synthesized by addition of NaBH₄ to a solution of HAuCl₄ and sodium citrate. Then AuNP@zPBYP and AuNP@PEG were prepared by

coating the polymers onto AuNP@citrate, followed by crosslinking of AuNP@zPBYP cysteines to form AuNP@X-zPBYP. Morphological analysis of the coated AuNPs revealed similarly sized cores of ca. 4 nm and increased hydrodynamic diameters of the polymer-coated AuNPs relative to the citrate-coated AuNPs. Degradation studies indicated hydrolysis of side chain and backbone units proceeded to an extent of ca. 75% over 2 d in nanopure water (pH 5-6) together with broadening and red-shifting of the SPR peak of AuNP@zPBYP over time. The coated NPs exhibited negligible immunotoxicity, as demonstrated by incubating RAW 264.7 mouse macrophages with the four AuNP formulations followed by measuring the levels of 23 cytokines relative to those in cells incubated without NPs. Cytokine adsorption studies showed that AuNP@zPBYP had the best antifouling performance. While the cross-linked AuNP@X-zPBYP nanostructures showed higher cytokine adsorption compared to their un-cross-linked counterparts, the low immunotoxicity of these materials suggests the biocompatibility of the cross-linking strategy. Future optimization of cross-linking degree will be conducted to balance NP stability and antifouling properties.

ASSOCIATED CONTENT

S Supporting Information

The Supporting Information is available free of charge on the ACS Publications website at DOI: 10.1021/acs.langmuir.8b02033.

Additional characterization and spectroscopic information including NMR spectra, TGA traces, FT-IR spectra, NMR spectra of degradation of zPBYP, identification of the side-chain moiety and monomeric repeat unit in the degradation products of zPBYP by ESI-MS analysis, and UV-vis spectra (PDF)

AUTHOR INFORMATION

Corresponding Author

*E-mail: wooley@chem.tamu.edu.

ORCID ®

Hai Wang: 0000-0002-1215-2613 Yongjian Liu: 0000-0002-1118-1535 Karen L. Wooley: 0000-0003-4086-384X

Author Contributions

The manuscript was written through the contributions of all authors, and all authors have approved the final version of the manuscript.

Author Contributions

R. Li and M. Elsabahy contributed equally.

Notes

The authors declare no competing financial interest.

ACKNOWLEDGMENTS

We gratefully acknowledge support from the National Science Foundation (CHE-1610311 and DMREF-1629094) and the Robert A. Welch Foundation through the W. T. Doherty-Welch Chair in Chemistry (A-0001). The Laboratory for Synthetic-Biologic Interactions (LSBI) at Texas A&M University is also gratefully acknowledged. We thank Dr. Fuwu Zhang and Dr. Jingwei Fan who provided insight and advice that greatly assisted the research.

REFERENCES

- (1) Hu, Y.; Mignani, S.; Majoral, J.-P.; Shen, M.; Shi, X. Construction of iron oxide nanoparticle-based hybrid platforms for tumor imaging and therapy. *Chem. Soc. Rev.* **2018**, *47*, 1874–1900.
- (2) Elzoghby, A. O.; Hemasa, A. L.; Freag, M. S. Hybrid protein-inorganic nanoparticles: From tumor-targeted drug delivery to cancer imaging. *J. Controlled Release* **2016**, 243, 303–322.
- (3) Palui, G.; Aldeek, F.; Wang, W.; Mattoussi, H. Strategies for interfacing inorganic nanocrystals with biological systems based on polymer-coating. *Chem. Soc. Rev.* **2015**, *44*, 193–227.
- (4) Wang, W.; Ji, X.; Du, L.; Mattoussi, H. Enhanced colloidal stability of various gold Nanostructures using a multicoordinating polymer coating. *J. Phys. Chem. C* **2017**, *121*, 22901–22913.
- (5) Karakoti, A. S.; Das, S.; Thevuthasan, S.; Seal, S. PEGylated inorganic nanoparticles. *Angew. Chem., Int. Ed.* **2011**, *50*, 1980–1994.
- (6) Joralemon, M. J.; McRae, S.; Emrick, T. PEGylated polymers for medicine: from conjugation to self-assembled systems. *Chem. Commun.* **2010**, *46*, 1377–1393.
- (7) Pelaz, B.; del Pino, P.; Maffre, P.; Hartmann, R.; Gallego, M.; Rivera-Fernandez, S.; de la Fuente, J. M.; Nienhaus, G. U.; Parak, W. J. Surface functionalization of nanoparticles with polyethylene glycol: Effects on protein adsorption and cellular uptake. *ACS Nano* **2015**, 9, 6996–7008.
- (8) Armstrong, J. K.; Hempel, G.; Koling, S.; Chan, L. S.; Fisher, T.; Meiselman, H. J.; Garratty, G. Antibody against poly(ethylene glycol) adversely affects PEG-asparaginase therapy in acute lymphoblastic leukemia patients. *Cancer* **2007**, *110*, 103–111.
- (9) Gaberc-Porekar, V.; Zore, I.; Podobnik, B.; Menart, V. Obstacles and pitfalls in the PEGylation of therapeutic proteins. *Curr. Opin. Drug Discovery Devel.* **2008**, *11*, 242.
- (10) Li, L.; Chen, S.; Jiang, S. Protein interactions with oligo(ethylene glycol) (OEG) self-assembled monolayers: OEG stability, surface packing density and protein adsorption. *J. Biomater. Sci., Polym. Ed.* **2007**, *18*, 1415–1427.
- (11) Li, B.; Yuan, Z.; Zhang, P.; Sinclair, A.; Jain, P.; Wu, K.; Tsao, C.; Xie, J.; Hung, H. C.; Lin, X.; Bai, T.; Jiang, S. Zwitterionic nanocages overcome the efficacy loss of biologic drugs. *Adv. Mater.* **2018**, *30*, 1705728.
- (12) Liu, Q.; Singha, P.; Handa, H.; Locklin, J. Covalent grafting of antifouling phosphorylcholine-based copolymers with antimicrobial nitric oxide releasing polymers to enhance infection-resistant properties of medical device coatings. *Langmuir* **2017**, *33*, 13105–13113.
- (13) Chen, X.; Lawrence, J.; Parelkar, S.; Emrick, T. Novel zwitterionic copolymers with dihydrolipoic acid: Synthesis and preparation of nonfouling nanorods. *Macromolecules* **2013**, *46*, 119–127.

- (14) Zhang, C.; Li, H.-N.; Du, Y.; Ma, M.-Q.; Xu, Z.-K. $CuSO_4/H_2O_2$ -triggered polydopamine/poly(sulfobetaine methacrylate) coatings for antifouling membrane surfaces. *Langmuir* **2017**, 33, 1210–1216.
- (15) Chen, S.; Li, L.; Zhao, C.; Zheng, J. Surface hydration: Principles and applications toward low-fouling/nonfouling biomaterials. *Polymer* **2010**, *51*, 5283–5293.
- (16) Elsabahy, M.; Li, A.; Zhang, F.; Sultan, D.; Liu, Y.; Wooley, K. L. Differential immunotoxicities of poly(ethylene glycol)-vs. poly (carboxybetaine)-coated nanoparticles. *J. Controlled Release* **2013**, 172, 641–652.
- (17) Pelegri-O'Day, E. M.; Paluck, S. J.; Maynard, H. D. Substituted polyesters by thiol—ene modification: rapid diversification for therapeutic protein stabilization. *J. Am. Chem. Soc.* **2017**, *139*, 1145—1154.
- (18) Steinbach, T.; Wurm, F. R. Poly(phosphoester)s: A new platform for degradable polymers. *Angew. Chem., Int. Ed.* **2015**, *54*, 6098–6108.
- (19) Schöttler, S.; Becker, G.; Winzen, S.; Steinbach, T.; Mohr, K.; Landfester, K.; Mailänder, V.; Wurm, F. R. Protein adsorption is required for stealth effect of poly(ethylene glycol)- and poly(phosphoester)-coated nanocarriers. *Nat. Nanotechnol.* **2016**, *11*, 372–377
- (20) Becker, G.; Ackermann, L.-M.; Schechtel, E.; Klapper, M.; Tremel, W.; Wurm, F. R. Joining two natural motifs: Catechol-containing poly(phosphoester)s. *Biomacromolecules* **2017**, *18*, 767–777.
- (21) Su, L.; Li, R.; Khan, S.; Clanton, R.; Zhang, F.; Lin, Y.-N.; Song, Y.; Wang, H.; Fan, J.; Hernandez, S. Chemical design of both a glutathione-sensitive dimeric drug guest and a glucose-derived nanocarrier host to achieve enhanced osteosarcoma lung metastatic anticancer selectivity. J. Am. Chem. Soc. 2018, 140, 1438–1446.
- (22) Zhang, S.; Zou, J.; Zhang, F.; Elsabahy, M.; Felder, S. E.; Zhu, J.; Pochan, D. J.; Wooley, K. L. Rapid and versatile construction of diverse and functional nanostructures derived from a polyphosphoester-based biomimetic block copolymer system. *J. Am. Chem. Soc.* **2012**, *134*, 18467–74.
- (23) Su, L.; Khan, S.; Fan, J.; Lin, Y.-N.; Wang, H.; Gustafson, T. P.; Zhang, F.; Wooley, K. L. Functional sugar-based polymers and nanostructures comprised of degradable poly(D-glucose carbonate)s. *Polym. Chem.* **2017**, *8*, 1699–1707.
- (24) Song, Y.; Chen, Y.; Su, L.; Li, R.; Letteri, R. A.; Wooley, K. L. Crystallization-driven assembly of fully degradable, natural product-based poly(L-lactide)-*block*-poly(α -D-glucose carbonate)s in aqueous solution. *Polymer* **2017**, *122*, 270–279.
- (25) Elsabahy, M.; Wooley, K. L. Data mining as a guide for the construction of cross-linked nanoparticles with low immunotoxicity *via* control of polymer chemistry and supramolecular assembly. *Acc. Chem. Res.* **2015**, *48*, 1620–1630.
- (26) Zhang, F.; Zhang, S.; Pollack, S. F.; Li, R.; Gonzalez, A. M.; Fan, J.; Zou, J.; Leininger, S. E.; Pavía-Sanders, A.; Johnson, R. Improving paclitaxel delivery: *In vitro* and *in vivo* characterization of PEGylated polyphosphoester-based nanocarriers. *J. Am. Chem. Soc.* 2015, 137, 2056–2066.
- (27) Zhang, S.; Zou, J.; Elsabahy, M.; Karwa, A.; Li, A.; Moore, D. A.; Dorshow, R. B.; Wooley, K. L. Poly(ethylene oxide)-block-polyphosphester-based paclitaxel conjugates as a platform for ultrahigh paclitaxel-loaded multifunctional nanoparticles. *Chem. Sci.* 2013, 4, 2122–2126.
- (28) Elsabahy, M.; Zhang, S.; Zhang, F.; Deng, Z. J.; Lim, Y. H.; Wang, H.; Parsamian, P.; Hammond, P. T.; Wooley, K. L. Surface charges and shell crosslinks each play significant roles in mediating degradation, biofouling, cytotoxicity and immunotoxicity for polyphosphoester-based nanoparticles. *Sci. Rep.* **2013**, *3*, 3313.
- (29) Her, S.; Jaffray, D. A.; Allen, C. Gold nanoparticles for applications in cancer radiotherapy: Mechanisms and recent advancements. *Adv. Drug Delivery Rev.* **2017**, *109*, 84–101.

(30) Zhang, S.; Li, A.; Zou, J.; Lin, L. Y.; Wooley, K. L. Facile synthesis of clickable, water-soluble, and degradable polyphosphoesters. *ACS Macro Lett.* **2012**, *1*, 328–333.

- (31) Jana, N. R.; Gearheart, L.; Murphy, C. J. Seeding growth for size control of 5–40 nm diameter gold nanoparticles. *Langmuir* **2001**, *17*, *6782*–*6786*.
- (32) Elsabahy, M.; Wooley, K. L. Reassessment of nanomaterials immunotoxicity. *Nano Today* **2018**, 20, 10–12.
- (33) Zhao, Y.; Detering, L.; Sultan, D.; Cooper, M. L.; You, M.; Cho, S.; Meier, S. L.; Luehmann, H.; Sun, G.; Rettig, M.; Dehdashti, F.; Wooley, K. L.; DiPersio, J. F.; Liu, Y. Gold nanoclusters doped with ⁶⁴Cu for CXCR4 positron emission tomography imaging of breast cancer and metastasis. *ACS Nano* **2016**, *10*, 5959–70.
- (34) Zhang, S.; Wang, H.; Shen, Y.; Zhang, F.; Seetho, K.; Zou, J.; Taylor, J.-S. A.; Dove, A. P.; Wooley, K. L. A simple and efficient synthesis of an acid-labile polyphosphoramidate by organobase-catalyzed ring-opening polymerization and transformation to polyphosphoester Ionomers by acid treatment. *Macromolecules* **2013**, *46*, 5141–5149.
- (35) Kabb, C. P.; Carmean, R. N.; Sumerlin, B. S. Probing the surface-localized hyperthermia of gold nanoparticles in a microwave field using polymeric thermometers. *Chem. Sci.* **2015**, *6*, 5662–5669.
- (36) Haiss, W.; Thanh, N. T.; Aveyard, J.; Fernig, D. G. Determination of size and concentration of gold nanoparticles from UV–Vis spectra. *Anal. Chem.* **2007**, *79*, 4215–4221.
- (37) Manson, J.; Kumar, D.; Meenan, B. J.; Dixon, D. Polyethylene glycol functionalized gold nanoparticles: the influence of capping density on stability in various media. *Gold Bull.* **2011**, *44*, 99–105.
- (38) Newman, J.; Blanchard, G. Formation of gold nanoparticles using amine reducing agents. *Langmuir* **2006**, 22, 5882–5887.
- (39) Sun, G.; Hagooly, A.; Xu, J.; Nyström, A. M.; Li, Z.; Rossin, R.; Moore, D. A.; Wooley, K. L.; Welch, M. J. Facile, efficient approach to accomplish tunable chemistries and variable biodistributions for shell cross-linked nanoparticles. *Biomacromolecules* **2008**, *9*, 1997–2006.